# Microfabricated Quadrupole Mass Spectrometer With a Brubaker Prefilter

Steven Wright, Shane O'Prey, Richard R. A. Syms, *Senior Member, IEEE*, Guodong Hong, and Andrew S. Holmes, *Member, IEEE*

***Abstract*—Microfabricated quadrupole mass spectrometers with Brubaker prefilters are demonstrated for the first time. Complete filters are assembled from two dies, each carrying two pairs of rods providing the prefilter and main filter sections. The rods are held in precision silicon mounts that are fabricated using wafer-scale deep reactive-ion etching and anodic bonding to glass substrates. Improvements to ion transmission are obtained by tuning the bias potential applied to the prefilter. The effect is explained in terms of a simple analytic theory for ion motion in the prefilter. Mass filtering with a range of $m/z = 0-1200$ and a resolution of $m/\Delta m \approx 150$ at 10% of peak height is demonstrated using 2–4-mm-long prefilter electrodes, 30-mm-long main electrodes (both of 650 $\mu$m diameter), and a radio-frequency drive at ≈6.5 MHz. [2009-0194]**

***Index Terms*—Mass spectrometry, microelectromechanical systems (MEMS), prefilter, quadrupole filter.**

## I. Introduction

THE QUADRUPOLE mass filter, originally introduced by Paul [1], is a workhorse of analytical mass spectrometry because it may easily be constructed without the need for a magnet. Its operation is well understood [2]–[4]. The device consists of a set of four parallel electrodes, arranged to create a hyperbolic electrostatic field, as shown in Fig. 1(a). Often, the ideal hyperbolic electrodes are approximated by cylinders of radius $r_e$ [5], with the ratio between $r_e$ and the radius of an inscribed circle $r_0$ being chosen to optimize performance [6], [7].

Ions are injected into a pupil between the electrodes, as shown in Fig. 1(b), and travel parallel to them for a distance $L_F$ under the influence of a time-varying field that contains both direct-current (dc) and alternating-current (ac) components. It can be shown that only ions near a particular mass-to-charge ratio will transit without discharging on a rod, and if the voltage amplitudes are ramped, the time variation of the output is a mass spectrum. Resolution is determined by the accuracy with which the field is created, the number of ac cycles experienced by each ion, and the ratio between the dc and ac voltages. Highly accurate construction is required to achieve an adequate analytical performance. The ions are injected with a small axial velocity, a radio-frequency (RF) drive is used, and the voltage ratio is chosen to operate near the peak of a so-called "first stability zone" [2]–[4].

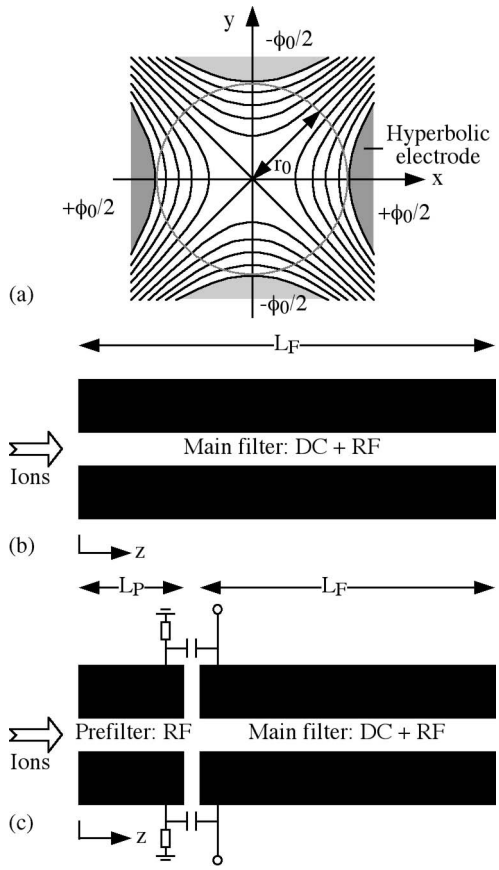


Fig. 1. (a) Hyperbolic electrostatic field. (b) Quadrupole. (c) Quadrupole with prefilter.

Sensitivity is primarily limited by the ion flux. Because the flux reduces as the size of the pupil is decreased, this aspect is clearly of importance to small mass spectrometers. However, sensitivity is also strongly reduced at high resolution due to the perturbing effect of the fringing field at the filter entrance caused by the exposed ends of the electrodes. In this region, the field is no longer purely hyperbolic and in addition contains axial components. In 1967, Brubaker proposed a simple solution, namely, to precede the filter with a short set of quadrupole electrodes or "stubbies" of length $L_P$ carrying only ac voltages, as shown in Fig. 1(c) [8]. The prefilter can be driven from the main filter via capacitors, using additional resistive pathways to ground to leak away any accumulated charge. Experimentally, very large improvements in transmission have been observed at

Manuscript received August 5, 2009; revised December 23, 2009. First published February 17, 2010; current version published April 2, 2010. Subject Editor G. Stemme.

S. Wright, S. O'Prey, and G. Hong are with Microsaic Systems Ltd., Surrey, GU21 5BX, U.K.

R. R. A. Syms and A. S. Holmes are with the Optical and Semiconductor Devices Group, Department of Electrical and Electronic Engineering, Imperial College London, London, SW7 2AZ, U.K. (e-mail: r.syms@imperial.ac.uk).

Digital Object Identifier 10.1109/JMEMS.2010.2040243

high resolution, albeit accompanied by mass-dependent transmission oscillations [9], [10].

The prefilter is itself a form of quadrupole known as an "RF-only quadrupole" [10], [11]. Such a device has its own set of detailed ion dynamics, which may be explained in terms of a confining potential well or "pseudopotential" created by an inhomogeneous time-varying electric field [12]. At low pressures, RF-only quadrupoles can be used for guiding or transporting ions, while at higher pressures, they can be used for additionally forcing ions toward the instrument axis by collision focusing [13], [14] and for fragmentation of ions by collision with a neutral gas [15]. The motion of ions through the prefilter and into the main filter is complicated and has so far mainly been understood in terms of detailed numerical simulations of trajectories [16], [17].

In recent years, considerable efforts have been devoted to miniaturization of most types of mass filter to allow portable or desktop applications [18]–[21]. Particular attention has been devoted to cylindrical ion traps (CITs) because these may be easily constructed as planar arrays [22]–[25], and several portable systems containing CITs have been demonstrated [26]–[29]. More recently, microfabricated ion traps have been demonstrated in cylindrical [30]–[33], toroidal [34], and linear [35]–[37] arrangements. Many other mass filter types have been realized in microfabricated form, including magnetic- and crossed-field filters [38]–[43], time-of-flight filters [44]–[48], and ion separators based on traveling electric fields [49], [50].

Quadrupole filters have been relatively difficult to miniaturize because their features are not amenable to fabrication by surface processing alone. Their size has been reduced to the millimeter scale using conventional engineering [51], and small quadrupole arrays have been constructed to increase sensitivity [52]–[54]. Unconventional fabrication methods, such as the LIGA process, have also been investigated for 100 micron-scale quadrupole arrays [55].

The most promising results have, however, been obtained from devices of intermediate size constructed using silicon-based microfabrication. Quadrupoles have been formed from two closely spaced stacked Si substrates, each containing pairs of 0.5-mm-diameter in-plane cylindrical electrodes rigidly fixed in V-grooves [56]–[59]. Similar array-type devices have also been proposed [60]. Taking advantage of the increased complexity offered by bonded silicon-on-insulator (BSOI), quadrupoles have been formed from two BSOI substrates that hold electrodes in grooves with micromachined springs [61], [62]. The latter arrangement has been used in portable and desktop mass spectrometers [63]. Alternative arrangements have used pairs of widely spaced substrates carrying out-of-plane cylindrical electrodes [64], [65], and in-plane arrangements of etched rods with rectangular cross section, operated in a higher stability zone [66]. The performance of microfabricated quadrupoles is steadily improving, but constructional accuracy has limited resolution, the maximum tolerated RF voltage has restricted mass range, and small size has restricted sensitivity.

One way to increase ion transmission in microfabricated quadrupoles would be to incorporate a prefilter. Unfortunately, none of the aforementioned approaches is appropriate due to the relatively short length of the filter electrodes. Out-of-plane constructions would clearly require complex stacked assemblies. In-plane approaches are potentially more suitable, but the V-groove construction in [56]–[59] suffers from RF coupling through the Si substrate, while the spring mounting used in [61], [62] is not easily adaptable to short electrodes.

In this paper, an enhancement to all major performance criteria of an in-plane microfabricated quadrupole is demonstrated by incorporating a Brubaker prefilter using an advanced fabrication process based on silicon on glass. The silicon parts are defined by deep reactive etching [67], [68] and attached to Pyrex by anodic bonding [69], [70] using methods previously developed for capacitive sensors [71] and vacuum packages [72]. The fabrication process is designed to improve yield by mounting the main electrodes on strain-relieved supports that reduce damage caused by thermal expansion mismatch. The use of glass substrates is designed to reduce RF coupling, so that higher voltages may be applied and the mass range may be increased. Finally, the incorporation of a prefilter is designed to increase transmission at high resolution.

A simple explanation of prefilter operation is presented in Section II in terms of an analytic theory of ion motion. The design and fabrication of the microfabricated filter are described in Section III. Mass filtering experiments are presented in Section IV, and a mass range of $m/z = 0{-}1200$ is demonstrated with a mass resolution of $m/\Delta m \approx 150$ at 10% of peak height using an RF drive at ≈6.5 MHz. The effects most commonly seen using a Brubaker prefilter (namely, an overall improvement in ion transmission, coupled with energy-dependent transmission effects) are all observed, and the experimental behavior is correlated to the earlier theoretical analysis. Finally, conclusions are drawn in Section V.

## II. Ion Motion in Quadrupole Filters and Prefilters

In general, the performance of quadrupole devices can only be understood from a detailed simulation of ion motion. Normally large numbers of ion trajectories are integrated, using a finite-element model of the electric fields that can incorporate fringe fields and coupling to an ion source [16], [17]. Here, the important features are highlighted using a simple analytic theory for noninteracting ions, assuming ideal hyperbolic fields.

### A. Electrostatic Field and Equations of Motion

The geometry is shown in Fig. 1. Assuming that axial and transverse motions are uncoupled and the axial energy is $V_A$, the axial velocity $v_A$ of an ion of mass $m$ and charge $e$ is

$$v_A = (2eV_A/m)^{1/2}. \tag{1}$$

The axial position $z$ may then be related to time $t$ as $z = v_A t$. Transverse motion is governed by the electric-field distribution shown in Fig. 1(a). Assuming that the electrodes carry potentials $\pm\phi_0/2$, the result is a 2-D potential field

$$\phi(x, y) = \phi_0(x^2 - y^2)/2r_0^2. \tag{2}$$

Here, $r_0$ is the radius of a circle touching the equipotentials $\phi = \pm\phi_0/2$. For an ion moving in the $z$-direction, the equations of motion in the $x$- and $y$-directions are

$$m\,d^2\mathrm{x}/dt^2 = -e\partial\phi/\partial x = -e\phi_0 x/r_0^2$$
$$m\,d^2y/dt^2 = -e\partial\phi/\partial y = +e\phi_0 y/r_0^2. \quad (3)$$

### B. Main Filter Operation

In the main filter, the applied voltage contains both dc and ac components, so that the time variation of the potential may be written as $\phi_0(t) = U - V\cos[\omega(t-t_0)]$, where $\omega = 2\pi f$ is an angular frequency, $\omega t_0$ is the starting phase of the ion, and $U$ and $V$ are constant potentials. In this case, the equations of motion reduce to

$$d^2x/dt^2 + \left(e/mr_0^2\right)\{U - V\cos[\omega(t-t_0)]\}\,x = 0$$
$$d^2y/dt^2 - \left(e/mr_0^2\right)\{U - V\cos[\omega(t-t_0)]\}\,y = 0. \quad (4)$$

Using substitutions $\zeta = \omega t/2$, $\zeta_0 = \zeta(0)$, $a = 4eU/(m\omega^2 r_0^2)$, and $q = 2eV/(m\omega^2 r_0^2)$, (4) can be reduced to Mathieu-like equations

$$d^2u/d\zeta^2 + \{a_u - 2q_u\cos[2(\zeta-\zeta_0)]\}\,u = 0 \quad (5)$$

where $u$ is $x$ or $y$, $a = a_x = -a_y$, and $q = q_x = -q_y$.

It can be shown (see, e.g., [3]) that the nature of the trajectory depends almost entirely on $a$ and $q$, varying little with initial conditions $u(0)$ and $u'(0)$ and starting phase $\zeta_0$. There are several regions on the $q-a$ plane that give rise to bounded stable solutions. The lower stability region is an approximately triangular region bounded by lines

$$a_0(q) = q^2/2 - 7q^4/128 + 29q^6/2304\ldots$$
$$b_1(q) = 1 - q - q^2/8 + q^3/64 - q^4/1536 - 11q^5/36\,864\ldots. \quad (6)$$

Line $a_0$ defines the stability limit for trajectories in the $y$-direction, while line $b_1$ is the same limit in the $x$-direction. Between the two, trajectories are stable in both directions. The apex of the stable region lies at $a = 0.23699$ and $q = 0.70600$, so that $U/V = a/2q = 0.1678$.

Fig. 2(a) shows sample $x$-trajectories obtained by numerical integration of (5), calculated assuming that $x(0) = 1$, $x'(0) = 0$, $\zeta_0 = 0$, $q = 0.706$, and $a/2q = 0.1671$ (thick line) and $a/2q = 0.1675$ (thin line). These two conditions lie just below the apex of the stability region. In each case, the motion involves rapid oscillations, whose amplitudes slowly increase first and then slowly decrease, so that the trajectory is bounded. However, for $a/2q = 0.1675$, the apex of the stable region is approached more closely, and the peak ion displacement is larger. Consequently, although the trajectory remains stable in this case, ions must be injected closer to the axis to transit successfully. Because the ions are injected as a relatively broad beam, the overall transmission is therefore likely to fall. As an extension, it may be assumed that perturbations to the direction of ions traveling close to the axis caused by fringe fields will also reduce transmission.

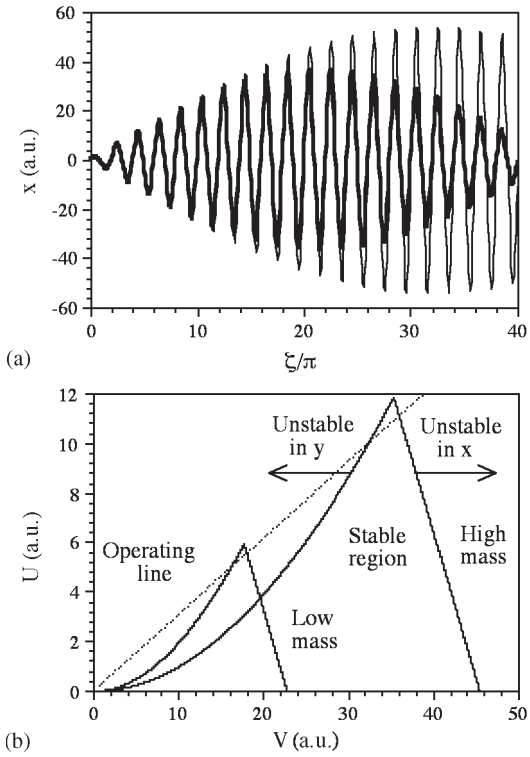


Fig. 2. (a) Sample $x$-trajectories in a main filter, calculated assuming that (thick line) $q = 0.706$, $\zeta_0 = 0$, and $a/2q = 0.1671$ and (thin line) $a/2q = 0.1675$. (b) Shape of the first stability zone, plotted on the $V-U$ plane for different masses.

In operation, $U$ and $V$ are normally ramped together, following an operating line passing just below the apex of the lower stability region of different masses, as shown in Fig. 2(b). Stable trajectories are then only obtained for a narrow mass range, so that the device acts as a scanning mass filter, with the filtered mass being determined from the ac voltage as $m = 2eV/(q\omega^2 r_0^2)$. The use of a scan line passing close to the stability tip requires that the voltage ratio $U/V$ be just less than 0.1678, with the mass resolution increasing as this value is approached. However, the previous discussion implies that there is a tradeoff between ion transmission and resolution, with the former falling as the latter rises. Based only on the width of the stable region, mass resolution $m/\Delta m$ can be estimated as [3]

$$m/\Delta m = 0.1256/\{0.1678 - U/V\}. \quad (7)$$

However, resolution is strongly affected by other factors, such as the number of RF cycles experienced by the ion, and constructional accuracy.

### C. Prefilter Operation

In the prefilter, the dc voltage is omitted, so that the equations of motion reduce to

$$d^2u/d\zeta^2 - 2q_u\cos[2(\zeta-\zeta_0)]\,u = 0. \quad (8)$$

This simplification causes a change in behavior, which may conveniently be discussed in terms of a simple approximation

developed for time-varying inhomogeneous fields [12]. The approximate solution is found by assuming that ion trajectories consist of a large mean trajectory $\xi_0(\zeta)$ combined with small oscillations $\xi_1(\zeta)\cos[2(\zeta-\zeta_0)]$ at the RF frequency. In this case, the complete ion displacement may be written as

$$u(\zeta) = \xi_0(\zeta) + \xi_1(\zeta)\cos\left[2(\zeta-\zeta_0)\right]. \tag{9}$$

Differentiating this solution, but assuming that the derivatives of $\xi_1$ can be neglected, yields

$$d^2u/d\zeta^2 \approx d^2\xi_0/d\zeta^2 - 4\xi_1\cos\left[2(\zeta-\zeta_0)\right]. \tag{10}$$

Substituting (9) and (10) into (8), but noting that $\cos^2(\theta) = \{1+\cos(2\theta)\}/2$, yields

$$d^2\xi_0/d\zeta^2 - 4\xi_1\cos\left[2(\zeta-\zeta_0)\right] - 2q_u\xi_0\cos\left[2(\zeta-\zeta_0)\right] - q_u\xi_1\left\{1+\cos\left[4(\zeta-\zeta_0)\right]\right\} = 0. \tag{11}$$

Separately equating the constant terms and the coefficients of $\cos[2(\zeta-\zeta_0)]$, but neglecting the term involving $\cos[4(\zeta-\zeta_0)]$ in (9), then gives

$$d^2\xi_0/d\zeta^2 - q_u\xi_1 = 0 \quad \xi_1 = -q_u\xi_0/2. \tag{12}$$

Verification that neglect of the higher order term is reasonable (at least within the limits of the initial approximation) can be achieved by including an additional term $\xi_2(\zeta)\cos[4(\zeta-\zeta_0)]$ in the assumed solution (9) and showing that its coefficient is small.

Finally, combining (12) shows that the mean trajectory is governed by the second-order differential equation

$$d^2\xi_0/d\zeta^2 + \left(q_u^2/2\right)\xi_0 = 0. \tag{13}$$

Because $q_u^2/2$ is constant, (13) describes simple harmonic motion and implies that the ion will oscillate to and fro in the form of potential well known as a "pseudopotential," which is proportional to the square of the applied RF voltage. The general solution for $\xi_0(\zeta)$ is

$$\xi_0(\zeta) = A\cos(q_u\zeta/\sqrt{2}) + B\sin(q_u\zeta/\sqrt{2}). \tag{14}$$

Equation (14) describes a sinusoidal trajectory with a constant amplitude and a period determined by the value of $q_u$, with a larger period being obtained at smaller $q_u$. Equation (12) implies, in turn, that the amplitude of the faster oscillations is not constant, but depends on the mean trajectory, so that the complete solution $u(\zeta)$ is

$$u(\zeta) = \{A\cos(q_u\zeta/\sqrt{2}) + B\sin(q_u\zeta/\sqrt{2})\} \times \{1-(q_u/2)\cos\left[2(\zeta-\zeta_0)\right]\}. \tag{15}$$

Although the period of the oscillation is the same for all ions, the exact trajectory depends on coefficients $A$ and $B$, which must be obtained from the boundary conditions. For example,

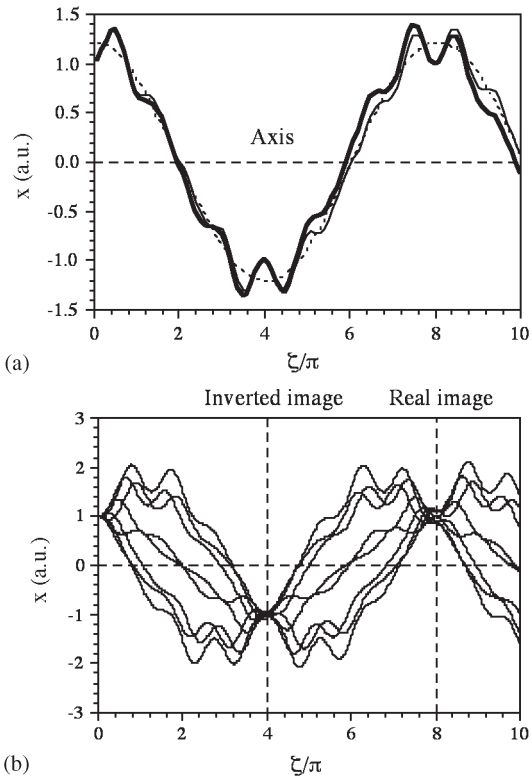


Fig. 3. (a) Example $x$-trajectories in a pre-filter, calculated assuming that $\zeta_0 = 0$ and $q = 0.35$. Thick lines show the exact solution, thin lines show the approximate solution, and dashed lines show the mean trajectory. (b) Exact trajectories, calculated assuming $q = 0.35$ and assuming different starting phases $\zeta_0 = \nu\pi/8$ with $\nu = 0, 1, \ldots 7$.

for ions injected parallel to the axis at a distance $u(0)$ from the axis, $A$ and $B$ are

$$A = u(0)/\left\{1-(q_u/2)\cos(2\zeta_0)\right\}$$
$$B = A\sqrt{2}\sin(2\zeta_0)/\left\{1-(q_u/2)\cos(2\zeta_0)\right\}. \tag{16}$$

In this case, Fig. 3(a) shows comparisons between the exact solution [(8)], the approximate solution [(15)], and the mean trajectory [(14)] for $x$-trajectories obtained with $\zeta_0 = 0$ and $q = 0.35$. Here, the exact and approximate solutions are in excellent agreement. The period of the main oscillation is large, the amplitude of the faster superimposed oscillation is small, and the mean trajectory is a good representation of the overall motion. When $q$ rises (for example, toward 0.706), the agreement becomes less good because the exact solution predicts a smaller mean period and larger superimposed oscillations. However, despite this discrepancy, a qualitatively similar behavior is obtained.

The operation of a Brubaker prefilter may now be understood in broad terms as follows. First, it provides an improvement in transmission by minimizing the effects of dc fringe fields at the sensitive input to the main filter. Second, it provides a guiding effect on the input ions, whose trajectories are forced by the pseudopotential to have an inherent periodicity.

When $q$ is sufficiently small, (12) implies that $\xi_1$ will be negligible. Only the slow oscillations need to be considered, and the solution is mainly described by (14) and (16). Because coefficient $B$ is strongly dependent on starting phase $\zeta_0$, ions

entering at different times must follow different trajectories. In particular, because $B > A$, ions entering near $\zeta_0 = \pi/4$ will make larger maximum excursions. However, whenever the sin term in (14) vanishes, the effect of the phase disappears. This condition occurs when

$$q_u\zeta/\sqrt{2} = \mu\pi, \qquad \text{where } \mu = 1, 2 \ldots. \tag{17}$$

The result is shown in Fig. 3(b), which shows exact ion trajectories calculated for different values of $\zeta_0$ equally distributed between zero and $\pi$, assuming that $q = 0.35$. The trajectories are significantly different, with much larger maximum excursions in some cases. However, all trajectories return together when $\zeta/\pi = \sqrt{2}/0.35 \approx 4.04$, $\zeta/\pi = 8.08$, and so on. In the former and latter cases, the prefilter is effectively forming an inverted and a real image of the input-ion distribution, respectively. Integrating over all possible starting conditions in both $x$- and $y$-directions, as was done by Trajber *et al.* [16], [17], the average diameter of the ion beam will clearly be smaller at the image conditions. If this point coincides with the start of the main filter, further benefits in transmission might be expected because ions will then be injected optimally through the dc fringe fields.

Substituting $\zeta = \omega t/2, t = L_P/v_A$, and $v_A = (2eV_A/m)^{1/2}$ into (17) yields the axial ion energy $V_A$ required to reach each of these image-forming conditions as

$$1/V_A^{1/2} = 2\mu(e/m)^{1/2}/(qfL_P). \tag{18}$$

Equation (18) now implies that mass-dependent transmission effects would be expected at fixed energy. Alternatively, fluctuations in transmission with energy would be expected for a fixed mass, so that a plot of $1/V_A^{1/2}$ against peak number $\mu$ should be a straight line.

To minimize the rate at which transmission changes with energy or mass, $\mu$ should be small. For example, if $\mu \approx 1$, the prefilter will operate near its primary image-forming condition, and quite-large changes in mass will be needed to reach the second one. To achieve a small value of $\mu$, either a large axial ion energy $V_A$ or a short prefilter length $L_P$ is required. Large ion energies are undesirable because small velocities are required for high resolution in the main filter. Consequently, $L_P$ is normally small. However, it cannot be too small, or the advantages of fringe-field screening will be lost. The exact choice is therefore a compromise, with $L_P$ typically being taken to be around the electrode diameter [8]. Unfortunately, in MEMS devices, there are difficulties with handling very short rods, and we have therefore investigated somewhat longer prefilters. Similarly, the exact choice of separation between the electrodes in the two filter sections is a compromise. The gap cannot be too large, or fringe fields will again be an issue. However, it cannot be too small, or breakdown may occur. The gap is therefore normally taken as a small fraction of the electrode diameter. Once again, there are additional difficulties in MEMS devices with reliably achieving small gaps and those used here were the minimum compatible with repeatable alignment.

The prefilter length $L_P$ is then normally a small fraction of the main filter length $L_F$. If both sections are directly coupled and driven using dc and RF, the combination acts as a marginally longer main filter. It might therefore be expected that some of the beneficial effects of the capacitively coupled RF-only prefilter will be masked by the improved resolution afforded by the longer directly coupled combined filter. However, [3, eq. (6.3)] shows that, given the stated operating parameters, the ultimate resolution is not limited in the present case by the number of cycles. Hence, this difference in filter length is of no consequence.

Departures from the previous predictions are to be expected at high resolution, as $q$ will then be large, or whenever the assumption of a parallel input beam is inappropriate, e.g., when the size of the entrance pupil is large compared with the exit pupil of the ion source.

## III. Design and Fabrication

Experience with early microfabricated quadrupoles has shown that accurate construction using materials that are appropriate for RF operation at up to several hundred volts is essential for high resolution. Previous comparable devices have used dies formed from oxidized silicon or BSOI to mount cylindrical electrode rods formed from metallized glass or stainless steel. Problems are then caused by the temperature rise that follows from RF heating within the semiconducting substrate, because the mismatch in thermal expansion coefficient of the electrodes and silicon causes die deformation and/or electrode detachment. Electrical loss also makes it difficult to achieve sufficiently high voltage from the RF drive.

### A. Design

Here, we introduce a new approach based on silicon on glass, which provides improved electrical, mechanical, and thermal performance. The complete mass filter is constructed from a pair of microfabricated dies, each carrying half of the electrode rods. Fig. 4(a) shows a single die, which provides microfabricated silicon mounts for pairs of prefilter and main filter electrodes on a glass substrate. Here, the aspect ratio has been reduced for clarity. The short prefilter electrodes are mounted in a single fixed silicon feature, as shown in Section A–A' of Fig. 4(b). However, the longer main filter electrodes must be held at each end. To allow differential thermal expansion with respect to the glass substrate, which otherwise tends to bend the substrate, one end of each electrode is held in a fixed feature, while the other is mounted in a spring feature formed as a suspended portal frame, as shown in Section B–B'. Associated with axial motion of the electrodes is a quadratically varying transverse motion that tends to separate their movable ends. Over a temperature range of, for example, 100°, the transverse motion is submicrometer for the flexure length used. Because this deflection is small compared with other dimensional tolerances, its effect on performance has not been quantified. However, because it varies quadratically with the inverse of flexure length, it could easily be reduced by design. The effect of thermal expansion between the electrodes and the very much shorter contact regions on the silicon parts is assumed to be small enough to allow attachment using conductive epoxy.

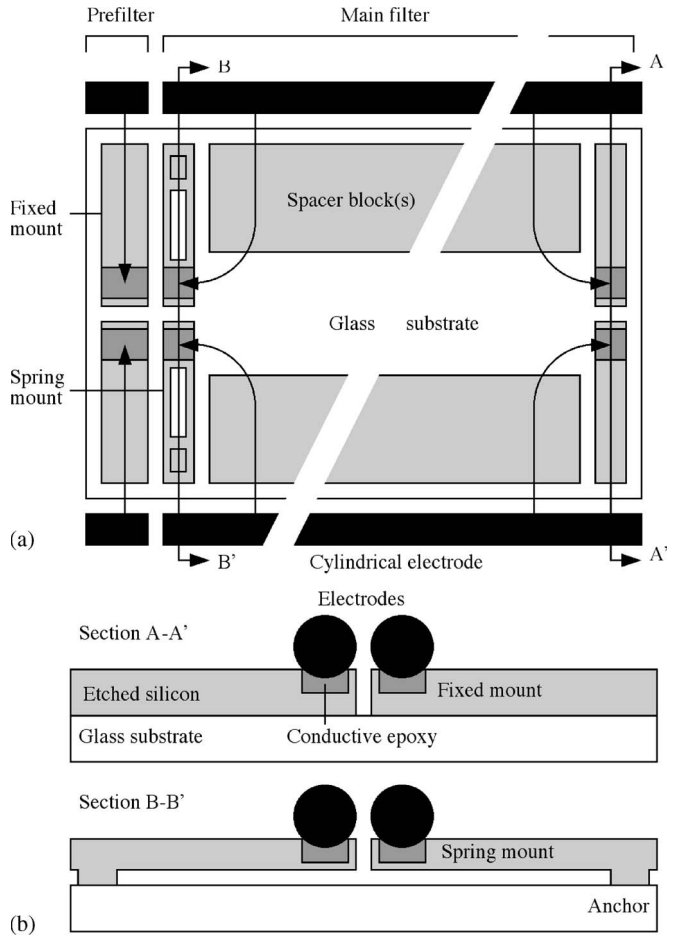


Fig. 4. (a) Plan and (b) section views of the microfabricated quadrupole die with Brubaker prefilter.

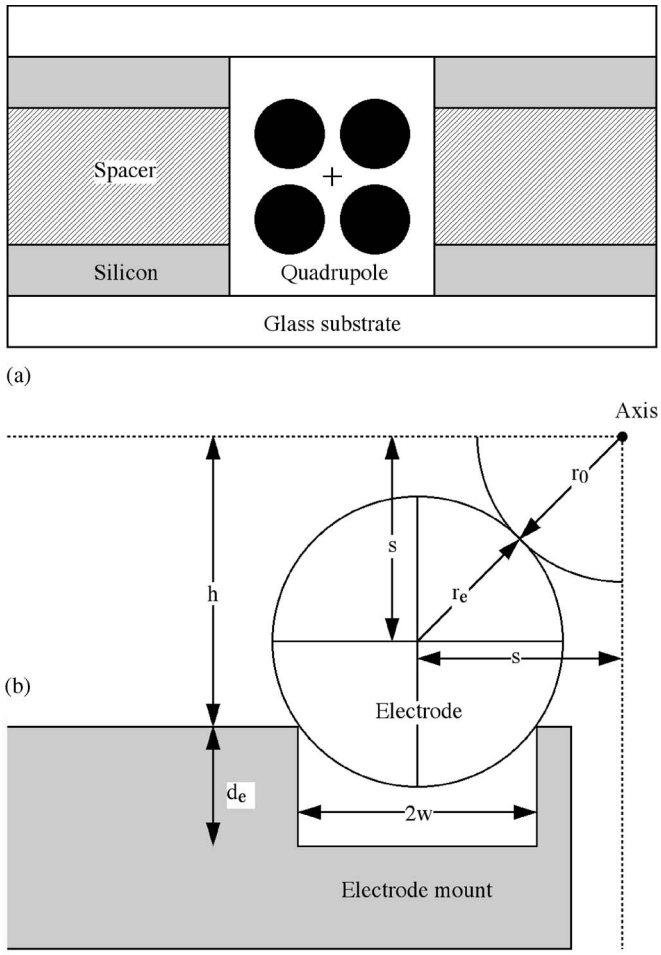


Fig. 5. (a) Quadrupole assembly. (b) Geometry for calculation of rod mount design parameters.

Silicon features also provide mounts for precision alignment spacers, which allow two such substrates to be aligned together in three orthogonal directions so that the combined set of electrodes forms a quadrupole, as shown in Fig. 5(a). The dimensions of the electrode-mounting fixtures can be calculated using the quadrant geometry shown in Fig. 5(b). For example, the distance $s$ between the electrode centers and the ion optical axis is $s = \{r_e + r_0\}/2^{1/2}$. If the distance between the two contact points of the cylindrical electrode and the groove in the supporting feature is $2w$, the height $h$ between the contact points and the axis of symmetry is $h = s + (r_e^2 - w^2)^{1/2}$. Suitable choices of $r_e$, $r_0$, $s$, $w$, and $h$ therefore allow the geometry of a quadrupole to be established. Other key dimensions, such as flexure widths and lengths, can be chosen to provide suitable thermal compliance.

### B. Fabrication

Devices were fabricated using a high-yield wafer-scale batch process based on 100-mm-diameter wafers of silicon and Pyrex glass, as shown in Fig. 6. The Si wafers were 400 $\mu$m thick, (100) oriented, D/S polished, and thermally matched to the glass wafers, which were typically 500-$\mu$m-thick Pyrex 7740 type. The silicon was repetitively patterned by mid-UV photolithography using a Quintel IR 4000 contact mask aligner equipped with through-wafer infrared illumination, and etched using a Surface Technology Systems Single-Chamber Multiplex inductively coupled plasma etcher operating a cyclic etch–passivation process based on $SF_6$ and $C_4F_8$ gases (the Bosch process). In each case, an AZ9260 photoresist was used for patterning, and a silicon etch rate of 1 $\mu$m/min was used for deep etching. The residual resist was stripped using an Oxford Plasma Technology System 80 RIE.

Three layers of patterning were used. The rear-side silicon was etched first to a shallow depth to define the anchor points for electrode mounts and form shallow recesses to allow subsequent motion of the suspended parts (Step 1). The main outlines of the electrode mounts were then partially defined using a second etch (Step 2). The wafer was then anodically bonded to a Pyrex wafer at the anchors, using an aligner–bonder (Step 3). A conducting surface layer was then provided on the front side using layers of Cr and Au metals deposited using a Nordiko RF sputter coater with thicknesses of 30 and 100 nm, respectively (Step 4). The metals were patterned by lithography and wet chemical etching in potassium iodide first and then in ceric ammonium nitrate (Step 5). The front-side silicon was then etched to complete the definition of the electrode mounts and form alignment trenches for the electrode rods (Step 6). In some variants, holes were formed in the glass prior to bonding to

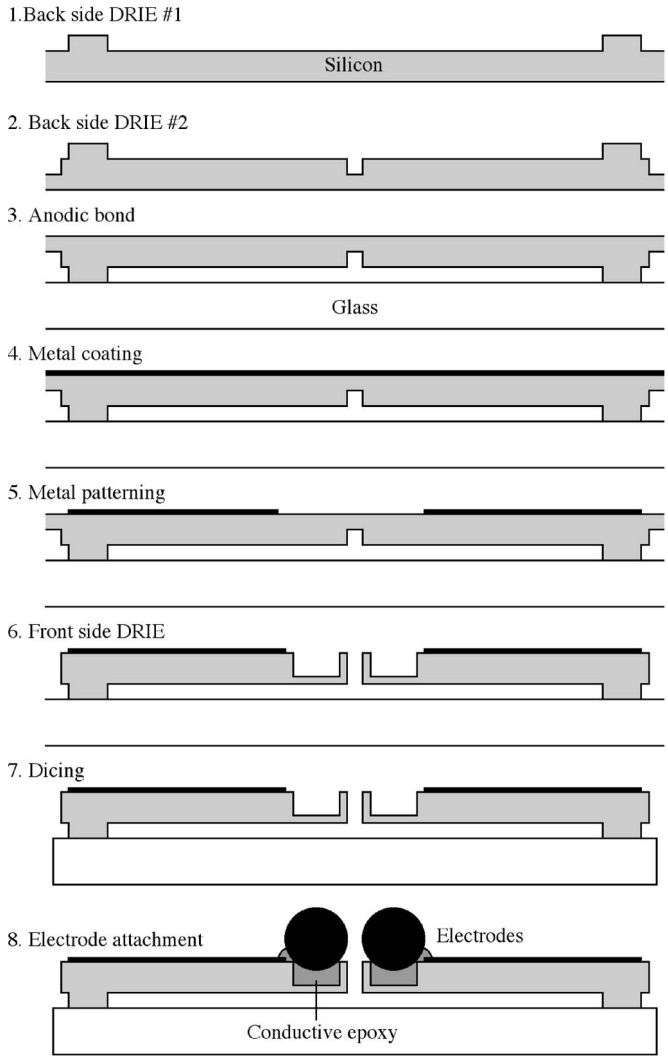


Fig. 6. Process flow for device fabrication.

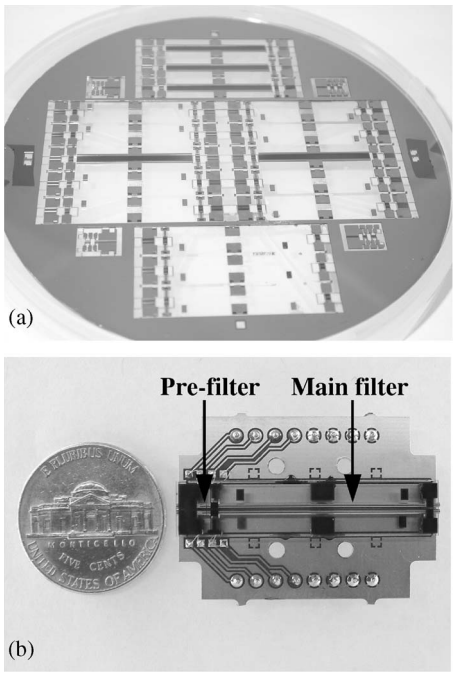


Fig. 7. (a) Silicon-on-glass wafer before dicing. (b) Assembled quadrupole filter with prefilter.

allow access to electrodes. However, the completed wafers were entirely robust. Fig. 7(a) shows a completed silicon-on-glass wafer before dicing. A variety of filter variants may be seen, each comprising a set of electrically isolated silicon parts on a glass backing, together with additional test structures. Finally, the wafer was mechanically diced using a rotary saw to yield dies of approximately 7 mm in width and 34 mm in length (Step 7), and the electrode rods were attached using conductive epoxy (Step 8).

Metal-coated glass electrodes have previously been used by one of the present authors [56], and these can have reduced mismatch in thermal expansion coefficient. However, they are tedious to fabricate because at least two coating cycles of each of the two metals (an adhesion layer and a conductor) are required to avoid breaks in the film. Stainless-steel electrodes are simpler to source, and the elastic suspension then provides an effective solution to thermal mismatch.

Stainless-steel electrode rods were purchased precut with a diameter of 650 $\mu$m. The rod ratio was $r_e/r_0 \approx 1.14$, and lengths of either 2 or 4 mm were used for the prefilter and 30 mm for the main filter. After cleaning, the rods were inserted into their respective alignment grooves and attached using conductive epoxy. Rods were inserted manually, and their longitudinal positions were adjusted under a microscope. Epoxy was again applied manually, and its amount was verified under the same microscope.

The design separation between the two filter sections was 80 $\mu$m. Using 80 measurements taken from 20 devices, the average axial separation between the prefilter and main filter electrodes was determined as 79.1 $\mu$m, with a standard deviation of 10.3 $\mu$m. Similarly, using 40 measurements taken from ten devices, the average axial displacement between two rod ends on the same die (measured for the main rod at the prefilter end) was determined as 5.3 $\mu$m, with a standard deviation of 5.6 $\mu$m.

No damage to the flexible electrode suspensions was observed despite the use of mechanical handling during assembly and thermal curing for the attachment epoxy. Connections were then made to the electrode mounts using gold wire and conductive epoxy. A second die was then stacked on top of the first, using the precision alignment spacers, and connections from the top die were then brought down to a small PCB submount. Fig. 7(b) shows an assembled filter. The prefilter is on the left, while the main filter is on the right. The electrode rods may be seen running along the center of the device.

## IV. Evaluation

The performance of the completed devices was evaluated using an electron-impact (EI) ion source and analytes that give well-separated mass peaks over a wide mass range. The overall aim was to demonstrate the advantages of using a silicon-on-glass technology and incorporating a prefilter with respect to improved mass range, resolution, and transmission.

### A. Experimental Arrangement

Mass filters were evaluated in a stainless-steel vacuum test rig pumped by a 130-ls$^{-1}$ turbo pump and equipped with a cold-cathode pressure gauge. Filters were mounted on stainless-steel flanges equipped with electrical feedthroughs between an EI ion source and a Channeltron electron multiplier used for ion detection.

The ion source is similar to the well-known VG Anavac source. It is designed for use with a much larger quadrupole filter (6-mm-diameter rods) and consequently produces a relatively large ion beam. The exit pupil of the final electrode of the ion source was therefore reduced to match the inscribed circle of the microfabricated filter. The ion energy in the main filter was determined from the voltage applied to the source cage, as the bias applied to the main rods was 0 V throughout. A Detech 2120 Channeltron (Detector Technology, Inc.) operated in pulse-counting mode was used to detect the ions.

RF waveforms were supplied to the mass filter under computer control by custom electronics. The two out-of-phase RF signals required to drive the filter sections were supplied by a resonant amplifier driven by an HP 33120A signal generator. Frequencies in the range of 6.2–6.9 MHz were used, depending on the exact device configuration. A dc command voltage (0–10 V) was used to set the RF amplitude during a scan. The prefilter rods were coupled to the main rods using 100-pF capacitors. Any bias voltage was applied to the prefilter pairs through high-value resistors. The fraction of the RF component coupled to the prefilter is close to unity, as the impedance of the capacitors is smaller compared with that of the bias resistors.

### B. Mass Range

Mass spectra were obtained for perfluorotributylamine or PFTBA ($C_{12}F_{27}N$, molecular weight of 671.09) and tris(perfluoroheptyl)-s-triazine ($C_3N_3[(CF_2)_6CF_3]_3$, molecular weight of 1185.22). PFTBA is often used to calibrate mass spectrometers fitted with EI sources. It has a relatively high vapor pressure at room temperature and was therefore held in a stainless-steel phial located outside the vacuum system and connected to it by a leak valve. After pumping away the air above the sample, PFTBA was admitted to the vacuum chamber to a pressure of $5 \times 10^{-7}$ torr. Tris(perfluoro-heptyl)-s-triazine is also used for calibration, particularly for instruments with a high mass range. It is a solid at room temperature and has a low vapor pressure. A small amount (20 mg) was placed in a stainless-steel cup directly in front of the ion source, where it sublimed at a rate that was sufficient to raise the chamber pressure to between $5 \times 10^{-7}$ and $1 \times 10^{-6}$ torr.

Figs. 8 and 9 show mass spectra for the two compounds, obtained using devices equipped with 4- and 2-mm prefilter electrodes, respectively. In each case, the ion energy was $V_A = 2$ eV, and no prefilter bias was used. These spectra were acquired over 10 min in both cases and represent multiple summed scans. The acquisition period was chosen so as to give good signal-to-noise levels for the smallest peaks in the spectra. The larger peaks can all be seen in a single scan (acquired in less than 30 s). Fig. 8(a) shows a measured spectrum for PFTBA, and Fig. 8(b) shows for comparison a reference spectrum from the National Institute of Standards and Technology (NIST) mass spectral database [72]. High-mass portions of the experimental data are shown plotted using expanded intensity scales. The reference spectrum is clearly well reproduced by the microfabricated filter, and the mass scale is linear. There are some discrepancies in relative peak heights (for example, the relatively low peak at $m/z = 219$). One explanation may be the mass-dependent ion transmission effects investigated hereinafter. However, resolved peaks may be seen up to $m/z = 614$. Fig. 9(a) and (b) shows experimental data and a NIST reference spectrum for tris(perfluoroheptyl)-s-triazine. Here, mass peaks can be seen up to almost $m/z = 1200$, and the very small peak at $m/z = 1185$ (shown in detail later on) indicates successful detection of the molecular ion. At 1200 a.m.u., the maximum voltage between adjacent rods was 770 V. These results represent an approximate trebling of the mass range obtained in [59] and [60] and confirm the benefits of the improved electrical properties of glass substrates.

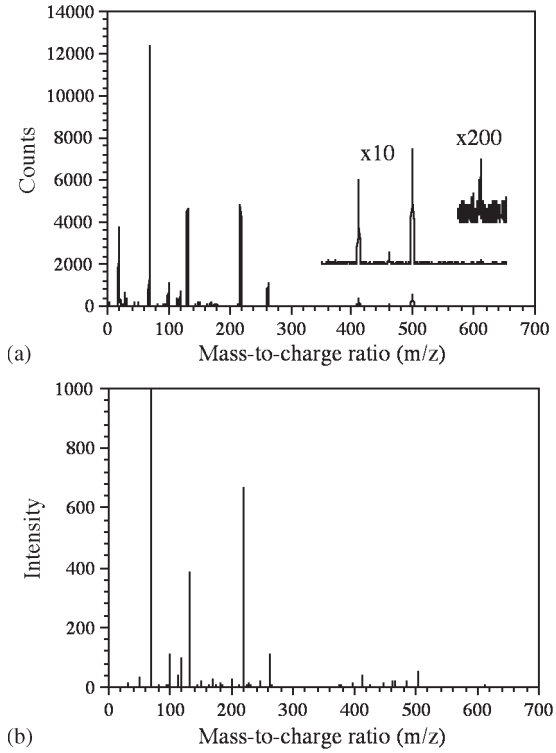


Fig. 8. Mass spectrum of perfluorotributylamine, as obtained using (a) a microfabricated quadrupole with prefilter and from (b) the NIST reference library.

### C. Mass Resolution

Fig. 10(a) shows the variation of the mass resolution $m/\Delta m$ (defined as the mass of the ion divided by the width of the peak, either at 10% or 50% of peak height) with voltage ratio $U/V$, measured at the $m/z = 219$ peak of PFTBA. The mass resolution rises steeply as the peak of the first stability zone is approached. Also shown in Fig. 10(a) is the theoretical

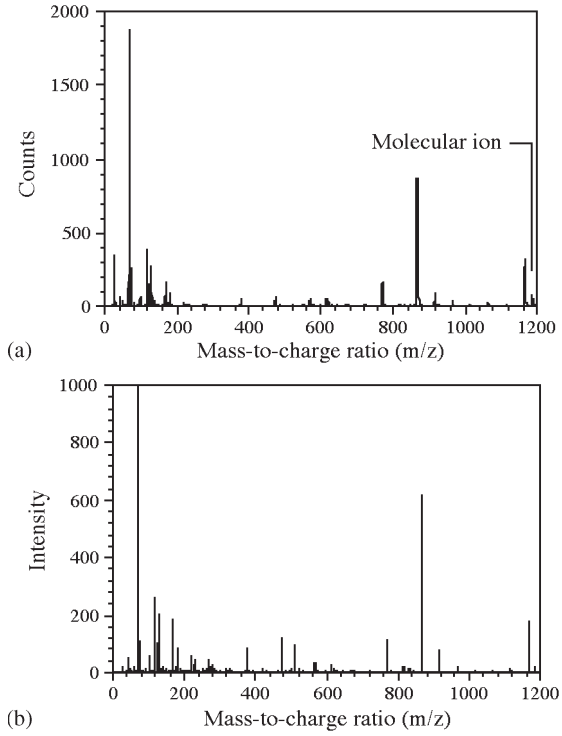


Fig. 9. Mass spectrum of tris(perfluoroheptyl)-s-triazine, as obtained using (a) a microfabricated quadrupole with prefilter and from (b) the NIST reference library.

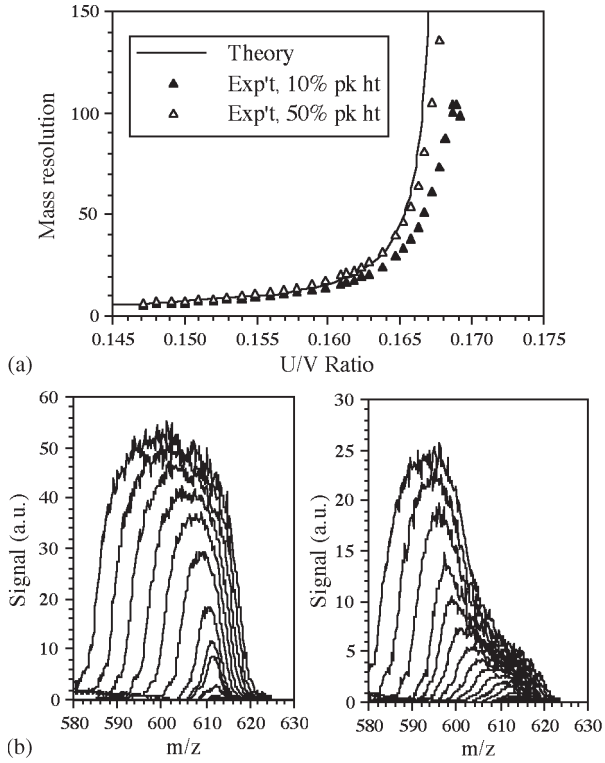


Fig. 10. (a) Variation of resolution $(m/\Delta m)$ with $U/V$ ratio. Points are experimental data for 10% and 50% of peak height; line is theory. (b) Peak shapes obtained for nominal $m/z = 614$ with an axial ion energy of 4 eV and different $U/V$ ratios, with (L) capacitive and (R) direct coupling to the prefilter.

prediction for the variation of resolution, as given in (7). The experimental data are in good agreement with the theory, suggesting that the fields in the quadrupole filter are reasonably close to ideal.

The beneficial effects of the prefilter can be seen in the peak shapes. Fig. 10(b) shows plots of the $m/z = 614$ peak of PFTBA obtained using a range of $U/V$ values and an ion energy of 4 eV. When the prefilter is capacitively coupled to the main filter and receives only the RF component of the waveform, the peak shape is uniform and collapses toward the high-mass side as the resolution increases. However, when the prefilter is directly coupled and fringing fields are reintroduced at the entrance to the filter, the peak shapes become asymmetric and collapse toward the high-mass shoulder as the resolution increases.

### *D. Ion Transmission*

Typically, the ion transmission of any quadrupole filter will fall as the resolution increases. For a well-constructed filter, transmission normally reduces quasi-linearly with resolution, when transmission is plotted on a logarithmic scale. However, at a maximum resolution that is often defined by some form of constructional imperfection (for example, misalignment of an electrode rod), transmission typically falls much more rapidly. The variation of transmission with resolution may even double back on itself and hence set a practical limit to the performance of the filter.

Fig. 11(a) shows the variation of transmission with resolution at 10% of peak height for the $m/z = 219$ and 502 peaks of PFTBA. A best resolution of $m/\Delta m \approx 140$ is achieved, which represents an approximate doubling of the resolution reported in [62]. The effect of the prefilter on performance is shown in Fig. 11(b). Two sets of data are shown. The hollow points show the results obtained using capacitive coupling of the drive voltages to the prefilter electrodes. In agreement with Fig. 11(a), the maximum resolution is ≈140. The solid points show the corresponding results obtained with direct coupling of the drive voltages to the prefilter electrodes. In this case, both sets of electrodes carry both dc and ac, and the device effectively acts as a slightly longer quadrupole. The maximum resolution achieved is 115, and the signal intensity is reduced by up to an order of magnitude. These results are qualitatively similar to the original findings of Brubaker [8], who showed that an RF-only prefilter could increase transmission at a given mass or alternatively increase the maximum resolution.

Fig. 12 shows expanded views of tris(perfluoroheptyl)-s-triazine peaks near $m/z = 866$ and $m/z = 1166$, obtained using 2-eV axial ion energy and a device with 2-mm prefilter electrodes. In Fig. 12(a), the peak width at 10% of peak height is 6.2 a.m.u., giving a mass resolution of $m/\Delta m \approx 140$. In Fig. 10(b), the peak width is 7 a.m.u., giving $m/\Delta m \approx 165$. The corresponding values at 50% of peak height are 350 and 360, respectively. These results confirm that a good mass resolution may be obtained over the whole of the mass range. Fig. 12(b) also shows an expanded view of the molecular ion peak.

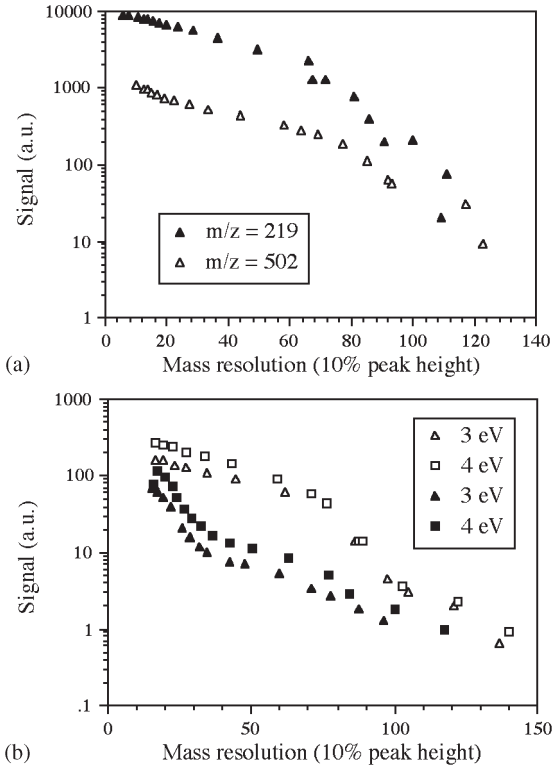


Fig. 11. (a) Variation of ion transmission with mass resolution for $m/z = 219$ and $m/z = 502$, with capacitive coupling of the prefilter and an axial ion energy of 2 eV. (b) Variation of ion transmission with resolution for (solid data points) direct and (hollow data points) capacitive coupling of the prefilter electrodes to the main electrodes. In each case, data were obtained for the $m/z = 614$ peak of PFTBA, using different axial ion energies.

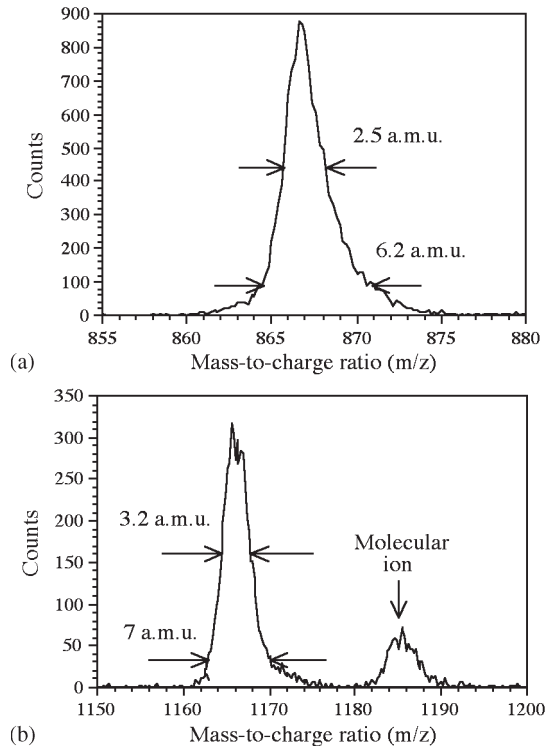


Fig. 12. High-resolution mass spectra for tris(perfluoroheptyl)-s-triazine, measured near (a) $m/z = 866$ and (b) $m/z = 1166$, using 2-eV axial ion energy.

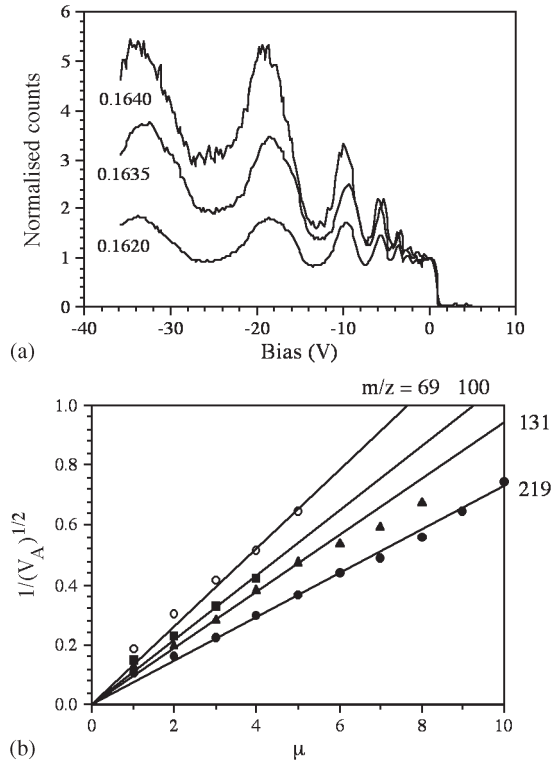


Fig. 13. (a) Variation of ion transmission with prefilter bias voltage, measured for the $m/z = 219$ peak of PFTBA for different $U/V$ ratios, as detailed on the legend. (b) Variation of $V_A$ with $\mu$ for the transmission maxima obtained for different fragment ions of PFTBA. Points are experimental data; lines are theory.

### *E. Transmission Oscillations*

Experience with macroscopic quadrupoles suggests that mass-dependent transmission effects will arise with a prefilter, which can cause inaccuracy in measurements of relative ion abundance. This possibility was investigated for the microfabricated device, using PFTBA. The ion-source cage voltage was fixed, the main filter was set to pass ions of a particular mass peak, and the ion transmission was measured as a function of a bias voltage applied to the prefilter electrodes. 22-MΩ bias resistors were used to ensure that the ac amplitude applied to the prefilter was closely tied to the ac voltage on the main filter.

Fig. 13(a) shows results obtained for the peak at $m/z = 219$ for different $U/V$ ratios. For each value of $U/V$, aperiodic oscillations in transmission can be seen, with the oscillation period reducing and overall transmission falling as the bias reduces. However, the locations of the peaks and troughs tend to particular values as $U/V$ rises and the peak of the stability zone is reached. The oscillations are significant. If the bias is set to a value that is coincident with a trough, the signal can be attenuated by as much as 50%. However, as can be seen in Fig. 9, if the bias is coincident with a peak, the transmission can be increased sixfold. Measurements carried out for other ions showed similar transmission oscillations, albeit with different peak and trough locations. To improve mass spectral fidelity, the bias voltage should be ramped as the mass spectrum is scanned, so that it is maintained at an optimum value for each mass.

However, the large bias resistor introduces a time constant that restricts the rate of scanning. This limitation is unimportant in applications involving a long acquisition time or in single-ion monitoring.

The elementary theory of ion focusing in an RF-only quadrupole presented in Section II suggested that if the peak locations are determined by particular values of $V_A$, a plot of $1/V_A^{1/2}$ against $\mu$, where $\mu$ is the peak number, should be a straight line with a slope $2(e/m)^{1/2}/(qfL_P)$. Fig. 13(b) shows the variation $V_A$ with $\mu$ obtained at the different masses indicated. The straight lines are the theoretical estimates, calculated assuming that $q = 0.706$ (the peak of the first stability zone), $f = 6.4$ MHz, and $L_P = 4$ mm, to correspond to the device used, and the discrete data points show the measured results. The qualitative agreement is excellent, confirming the earlier interpretation of prefilter operation and suggesting that the overall behavior of the microfabricated device is indeed as expected. The rapidity of the transmission oscillations should reduce as the length of the prefilter section is reduced, and certainly, a reduction in $L_P$ down to ≈1 mm seems entirely practical.

## V. Conclusion

A new technology for microfabricated quadrupole mass filters has been developed using an advanced silicon-on-glass process based on a combination of deep reactive-ion etching and anodic bonding. A wafer-scale batch fabrication process for quadrupole filter dies has been demonstrated, which yields precision alignment features for pairs of electrode rods and spacers in the form of electrically isolated metallized silicon parts on glass substrates. Stainless-steel electrode rods are inserted into silicon mountings, and complete filters are assembled as a stacked combination of two dies separated by spacers. The improved electrical isolation of glass allows an inherently larger mass range than that with previous filters constructed on silicon and bonded silicon substrates, and a mass range of 0–1200 a.m.u. has been demonstrated with a resolution of ≈150 at ≈6.5-MHz frequency, the best performance of any form of microfabricated mass filter to date. The technology supports the incorporation of multiple electrode sections, allowing advantage to be taken of the improved transmission obtained when a short RF-only prefilter is combined with a main filter. Many of the characteristics of macroscopic prefilters have been observed, including improved transmission at high resolution and mass-dependent transmission. These improvements in performance suggest that benchtop mass spectrometers based on microfabricated filters are now a realistic possibility.

## Acknowledgment

The authors would like to thank P. Edwards and A. Finlay for their support and encouragement, and A. Malcolm for his technical assistance. The authors would also like to thank Applied Microengineering Ltd. and Loadpoint Ltd. for their assistance in wafer bonding and dicing, respectively.

## References

[1] W. Paul and H. Steinwedel, "Ein neues massenspektrometer ohne magnetfeld," *Z. Naturforschung*, vol. 8a, pp. 448–450, 1953.
[2] J. H. Batey, "Quadrupole gas analysers," *Vacuum*, vol. 37, no. 8/9, pp. 659–668, Sep. 1987.
[3] P. H. Dawson, *Quadrupole Mass Spectrometry and Its Applications*. Amsterdam, The Netherlands: Elsevier, 1976.
[4] P. H. Dawson, "Quadrupole mass analyzers: Performance, design and some recent applications," *Mass Spectrom. Rev.*, vol. 5, no. 1, pp. 1–37, Mar. 2005.
[5] P. H. Dawson and N. R. Whetten, "Quadrupole mass filter: Circular rods and peak shapes," *J. Vac. Sci. Technol.*, vol. 7, no. 3, pp. 440–441, May 1970.
[6] J. R. Gibson and S. Taylor, "Numerical investigation of the effect of electrode size on the behaviour of quadrupole mass filters," *Rapid Commun. Mass Spectrom.*, vol. 15, no. 20, pp. 1960–1964, Oct. 2001.
[7] D. J. Douglas and N. V. Konenkov, "Influence of the 6th and 10th spatial harmonics on the peak shape of a quadrupole mass filter with round rods," *Rapid Commun. Mass Spectrom.*, vol. 16, no. 15, pp. 1425–1431, Aug. 2002.
[8] W. M. Brubaker, "An improved quadrupole mass analyzer," *Adv. Mass Spectrom.*, vol. 4, pp. 293–299, 1968.
[9] W. Arnold, "Influence of segmented rods and their alignment on the performance of a quadrupole mass spectrometer," *J. Vac. Sci. Technol.*, vol. 7, no. 1, pp. 191–194, Jan. 1970.
[10] P. E. Miller and D. M. Bonner Denton, "The transmission properties of an RF-only quadrupole mass filter," *Int. J. Mass Spectrom. Ion Process.*, vol. 72, no. 3, pp. 223–238, Oct. 1986.
[11] P. H. Dawson, "Performance characteristics of an RF-only quadrupole," *Int. J. Mass Spectrom. Ion Process.*, vol. 67, no. 3, pp. 267–276, Nov. 1985.
[12] D. Gerlich, "Inhomogeneous RF fields: A versatile tool for the study of processes with slow ions," in *State-Selected and State-to-State Ion-Molecule Reaction Dynamics. Part 1: Experiment*, vol. LXXXII, *Adv. Chem. Phys.*, C. Y. Ng and M. Baer, Eds. New York: Wiley, 1992.
[13] D. J. Douglas and J. B. French, "Collision focusing effects in radio-frequency quadrupoles," *J. Amer. Soc. Mass Spectrom.*, vol. 3, no. 4, pp. 398–408, May 1992.
[14] A. V. Tolmachev, I. V. Chernushevich, A. F. Dodonov, and K. G. Standing, "A collision focusing ion guide for coupling an atmospheric pressure ion source to a mass spectrometer," *Nucl. Instrum. Methods Phys. Res. B, Beam Interact. Mater. At.*, vol. 124, no. 1, pp. 112–119, Apr. 1997.
[15] D. Gerlich, "Application of RF fields and collision dynamics in atomic mass spectrometry," *J. Anal. At. Spectrom.*, vol. 19, no. 5, pp. 581–590, May 2004.
[16] C. Trajber, M. Simon, and M. Csatlos, "On the use of prefilters in quadrupole mass spectrometers," *Meas. Sci. Technol.*, vol. 2, no. 8, pp. 785–787, Aug. 1991.
[17] C. Trajber, M. Simon, and S. Bohatka, "A method for uniform optimisation of quadrupole prefilters," *Rapid Commun. Mass Spectrom.*, vol. 6, no. 7, pp. 459–462, Jul. 1992.
[18] E. R. Badman and R. G. Cooks, "Special feature: Perspective—Miniature mass analysers," *J. Mass Spectrom.*, vol. 35, pp. 659–671, Jun. 2000.
[19] R. R. A. Syms, "Miniaturized mass spectrometers," presented at the 59th Annu. Pittsburgh Conf. Analytical Chemistry Applied Spectroscopy, New Orleans, LA, 2008.
[20] Z. Ouyang and R. G. Cooks, "Miniature mass spectrometers," *Annu. Rev. Anal. Chem.*, vol. 2, pp. 187–214, Jul. 2009.
[21] R. R. A. Syms, "Advances in microfabricated mass filters," *Anal. Bioanal. Chem.*, vol. 393, no. 2, pp. 427–429, Jan. 2009.
[22] R. G. Brewer, R. G. Devoe, and R. Kallenbach, "Planar ion microtraps," *Phys. Rev. A, Gen. Phys.*, vol. 46, no. 11, pp. R6 781–R6 784, Dec. 1992.
[23] J. M. Wells, E. R. Badman, and R. G. Cooks, "A quadrupole ion trap with cylindrical geometry operated in the mass-selective instability mode," *Anal. Chem.*, vol. 70, no. 3, pp. 438–444, Jan. 1998.
[24] O. Kornienko, P. T. A. Reilly, W. B. Whitten, and J. M. Ramsey, "Micro ion trap mass spectrometry," *Rapid Commun. Mass Spectrom.*, vol. 13, no. 1, pp. 50–53, Jan. 1999.
[25] E. R. Badman and R. G. Cooks, "A parallel miniature cylindrical ion trap array," *Anal. Chem.*, vol. 72, no. 14, pp. 3291–3297, Jul. 2000.
[26] G. E. Patterson, A. J. Guymon, L. S. Riter, M. Everly, J. Griep-Raming, B. C. Laughlin, Z. Ouyang, and R. G. Cooks, "Miniature cylindrical ion trap mass spectrometer," *Anal. Chem.*, vol. 74, no. 24, pp. 6145–6153, Dec. 2002.

[27] O. J. Orient and A. Chutjian, "A compact, high-resolution Paul ion trap mass spectrometer with electron-impact ionization," *Rev. Sci. Instrum.*, vol. 73, no. 5, pp. 2157–2160, May 2002.
[28] A. M. Tabert, J. Griep-Raming, A. J. Guymon, and R. G. Cooks, "High-throughput miniature cylindrical ion trap array mass spectrometer," *Anal. Chem.*, vol. 75, no. 21, pp. 5656–5664, Nov. 2003.
[29] M. Yang, T. Y. Kim, H.-C. Hwang, S.-K. Yi, and D.-H. Kim, "Development of a palm portable mass spectrometer," *J. Amer. Soc. Mass Spectrom.*, vol. 19, no. 10, pp. 1442–1448, Oct. 2008.
[30] M. G. Blain, L. S. Riter, D. Cruz, D. E. Austin, G. Wu, W. R. Plass, and R. G. Cooks, "Towards the hand-held mass spectrometer: Design considerations, simulation, and fabrication of micrometer-scaled cylindrical ion traps," *Int. J. Mass Spectrom.*, vol. 236, no. 1–3, pp. 91–104, Aug. 2004.
[31] S. Pau, C. S. Pai, Y. L. Low, J. Moxom, P. T. A. Reilly, W. B. Whitten, and J. M. Ramsey, "Microfabricated quadrupole ion trap for mass spectrometer applications," *Phys. Rev. Lett.*, vol. 96, no. 12, p. 120 801, Mar. 2006.
[32] F. H. W. Van Amerom, A. Chaudhary, M. Cardenas, J. Bumgarner, and R. T. Short, "Microfabrication of cylindrical ion trap mass spectrometer arrays for handheld chemical analyzers," *Chem. Eng. Commun.*, vol. 195, no. 2, pp. 98–114, Feb. 2008.
[33] A. Chaudhary, F. H. W. Van Amerom, and R. T. Short, "Development of microfabricated cylindrical ion trap mass spectrometer arrays," *J. Microelectromech. Syst.*, vol. 18, no. 2, pp. 442–448, Apr. 2009.
[34] D. E. Austin, M. Wang, S. E. Tolley, J. D. Maas, A. R. Hawkins, A. L. Rockwood, H. D. Tolley, E. D. Lee, and M. L. Lee, "Halo ion trap mass spectrometer," *Anal. Chem.*, vol. 79, no. 7, pp. 2927–2932, Apr. 2007.
[35] M. J. Madsen, W. K. Hensinger, D. Stick, J. A. Ratschuk, and C. Monroe, "Planar ion trap geometry for microfabrication," *Appl. Phys. B, Lasers Opt.*, vol. 78, no. 5, pp. 639–651, Mar. 2004.
[36] D. Stick, W. K. Hensinger, S. Olmschenk, M. J. Madsen, K. Schwab, and C. Monroe, "Ion trap in a semiconductor chip," *Nat. Phys.*, vol. 2, no. 1, pp. 36–39, Jan. 2006.
[37] M. Brownnutt, G. Wilpers, P. Gill, R. C. Thompson, and A. G. Sinclair, "Monolithic microfabricated ion trap chip design for scaleable quantum processors," *New J. Phys.*, vol. 8, p. 232, Oct. 2006.
[38] C. B. Freidhoff, "Mass spectrograph on a chip," in *Proc. IEEE Aerosp. Conf.*, 1997, p. 32.
[39] C. B. Freidhoff, R. M. Young, S. Sriram, T. T. Braggins, T. W. O'Keefe, J. D. Adam, H. C. Nathanson, R. R. A. Syms, T. J. Tate, M. M. Ahmad, S. Taylor, and J. Tunstall, "Chemical sensing using non-optical microelectromechanical systems," *J. Vac. Sci. Technol.*, vol. A17, no. 4, pp. 2300–2307, Jul. 1999.
[40] J. A. Diaz, C. F. Giese, and W. R. Gentry, "Sub-miniature E x B sector-field mass spectrometer," *J. Amer. Soc. Mass Spectrom.*, vol. 12, no. 6, pp. 619–632, Jun. 2001.
[41] J. A. Diaz, P. Daley, R. Miles, H. Rohrs, and D. Polla, "Integration test of a miniature ExB mass spectrometer with a gas chromatograph for development of a low-cost, portable, chemical detection system," *Trends Anal. Chem.*, vol. 23, no. 4, pp. 314–321, Apr. 2004.
[42] N. Sillon and R. Baptist, "Micromachined mass spectrometer," *Sens. Actuators B, Chem.*, vol. 83, no. 1–3, pp. 129–137, Mar. 2002.
[43] K. H. Gilchrist, C. A. Bower, M. R. Lueck, J. R. Piascik, B. R. Stoner, S. Natarajan, C. B. Parker, and J. T. Glass, "A novel ion source and detector for a miniature mass spectrometer," in *Proc. IEEE Sens. Conf.*, 2007, pp. 1372–1375.
[44] H. J. Yoon, J. H. Kim, T. G. Park, S. S. Yang, and K. W. Jung, "The test of hot emission for the micro mass spectrometer," *Proc. SPIE*, vol. 4408, pp. 360–367, Apr. 2001.
[45] H. J. Yoon, J. H. Kim, E. S. Choi, S. S. Yang, and K. W. Jung, "Fabrication of a novel micro time-of-flight mass spectrometer," *Sens. Actuators A, Phys.*, vol. 97/98, pp. 441–447, Apr. 2002.
[46] J. S. Hwang, S. W. Park, J. B. Cho, K. S. Oh, S. S. Yang, S. Lee, K. H. Koh, and K. W. Jung, "The micro mass spectrometer with a carbon nanostructure ion source," in *Proc. 1st IEEE Int. Conf. Nano/Micro Engineered Mol. Syst.*, 2006, pp. 1220–1223.
[47] G. F. Verbeck, R. Saini, J. W. Wylde, K. Tsui, and M. Ellis, "MEMS assembled mass spectrometry: A novel approach to miniaturization and construction of electron and ion optics," presented at the 54th ASMS Conf. Mass Spectrometry, Seattle, WA, 2006.
[48] E. Wapelhorst, J.-P. Hauschild, and J. Müller, "Complex MEMS: A fully integrated TOF micro mass spectrometer," *Sens. Actuators A, Phys.*, vol. 138, no. 1, pp. 22–27, Jul. 2007.
[49] P. Siebert, G. Petzold, A. Hellenbart, and J. Müller, "Surface microstructure/miniature mass spectrometer: Processing and applications," *Appl. Phys.*, vol. A67, no. 2, pp. 155–160, Aug. 1998.
[50] J.-P. Hauschild, E. Wapelhorst, and J. Müller, "Mass spectra measured by a fully integrated MEMS mass spectrometer," *Int. J. Mass Spectrom.*, vol. 264, no. 1, pp. 53–60, Jun. 2007.
[51] D. H. Holkeboer, T. L. Karandy, F. C. Currier, L. C. Frees, and R. E. Ellefson, "Miniature quadrupole residual gas analyser for process monitoring at milliTorr pressures," *J. Vac. Sci. Technol.*, vol. A16, no. 3, pp. 1157–1162, May 1998.
[52] R. J. Ferran and S. Boumsellek, "High-pressure effects in miniature arrays of quadrupole analyzers for residual gas analysis from $10^{-9}$ to $10^{-2}$ Torr," *J. Vac. Sci. Technol.*, vol. A14, no. 3, pp. 1258–1264, May/Jun. 1996.
[53] O. J. Orient, A. Chutjian, and V. Garkanian, "Miniature, high-resolution, quadrupole mass-spectrometer array," *Rev. Sci. Instrum.*, vol. 68, no. 3, pp. 1392–1397, Mar. 1997.
[54] S. Boumsellek and R. J. Ferran, "Tradeoffs in miniature quadrupole designs," *J. Amer. Soc. Mass Spectrom.*, vol. 12, no. 6, pp. 633–640, Jun. 2001.
[55] D. Wiberg, N. V. Myung, B. Eyre, K. Shcheglov, O. J. Orient, E. Moore, and P. Munz, "LIGA fabricated two-dimensional quadrupole array and scroll pump for miniature gas chromatograph/mass spectrometer," *Proc. SPIE*, vol. 4878, pp. 8–13, Dec. 2003.
[56] R. R. A. Syms, T. J. Tate, M. M. Ahmad, and S. Taylor, "Fabrication of a microengineered quadrupole electrostatic lens," *Electron. Lett.*, vol. 32, no. 22, pp. 2094–2095, Oct. 1996.
[57] S. Taylor, J. J. Tunstall, R. R. A. Syms, T. J. Tate, and M. M. Ahmad, "Initial results for a quadrupole mass spectrometer with a silicon micromachined mass filter," *Electron. Lett.*, vol. 34, no. 6, pp. 546–547, Mar. 1998.
[58] R. R. A. Syms, T. J. Tate, M. M. Ahmad, and S. Taylor, "Design of a microengineered quadrupole electrostatic lens," *IEEE Trans. Electron Devices*, vol. 45, no. 11, pp. 2304–2311, Nov. 1998.
[59] S. Taylor, J. J. Tunstall, J. H. Leck, R. F. Tindall, J. P. Jullien, J. Batey, R. R. A. Syms, T. J. Tate, and M. M. Ahmad, "Performance improvements for a miniature quadrupole with a micromachined mass filter," *Vacuum*, vol. 53, no. 1/2, pp. 203–206, May 1999.
[60] L. Lebel, L. F. Velasquez-Garcia, and A. I. Akinwande, "Arrays of microfabricated quadrupole mass filters," in *Tech. Dig. 18th Int. Vacuum Nanoelectronics Conf.*, 2005, pp. 366–367.
[61] M. Geear, R. R. A. Syms, S. Wright, and A. S. Holmes, "Monolithic MEMS quadrupole mass spectrometers by deep silicon etching," *J. Microelectromech. Syst.*, vol. 14, no. 5, pp. 1156–1166, Oct. 2005.
[62] S. Wright, R. R. A. Syms, S. O'Prey, G. Hong, and A. S. Holmes, "Comparison of ion coupling strategies for a microengineered quadrupole mass spectrometer," *J. Amer. Soc. Mass Spectrom.*, vol. 20, no. 1, pp. 146–156, Jan. 2009.
[63] A. Finlay, R. R. A. Syms, S. Wright, and A. Malcolm, "Microsaic Ionchip: The first commercially available mass spectrometer chip," presented at the 57th Annu. Pittsburgh Conf. Analytical Chemistry Applied Spectroscopy, Orlando, FL, 2006.
[64] L. F. Velasquez-Garcia and A. I. Akinwande, "An out-of-plane MEMS quadrupole for a portable mass spectrometer," in *Proc. TRANSDUCERS Conf.*, 2007, pp. 2315–2320.
[65] L. F. Velasquez-Garcia, K. Cheung, and A. I. Akinwande, "An application of 3D MEMS packaging: Out-of-plane quadrupole mass filters," *J. Microelectromech. Syst.*, vol. 17, no. 6, pp. 1430–1438, Dec. 2008.
[66] K. Cheung, L. F. Velasquez-Garcia, and A. I. Akinwande, "First principles optimization of mass produced microscaled linear quadrupoles for operation in higher stability regions," in *Tech. Dig. 20th IEEE Int. Vacuum Nanoelectronics Conf.*, 2007, pp. 214–215.
[67] M. Esashi, M. Takinami, Y. Wakabayashi, and K. Minami, "High rate directional deep dry etching for bulk silicon micromachining," *J. Micromech. Microeng.*, vol. 5, no. 1, pp. 5–10, Mar. 1995.
[68] A. M. Hynes, H. Ashraf, J. K. Bhardwaj, J. Hopkins, I. Johnston, and J. N. Shepherd, "Recent advances in silicon etching for MEMS using the ASE process," *Sens. Actuators A, Phys.*, vol. 74, no. 1–3, pp. 13–17, Apr. 1999.
[69] T. Rogers, "Considerations of anodic bonding for capacitive type silicon/glass sensor fabrication," *J. Micromech. Microeng.*, vol. 2, no. 3, pp. 164–166, Sep. 1992.
[70] A. Cozma and B. Puers, "Characterization of the electrostatic bonding of silicon and Pyrex glass," *J. Micromech. Microeng.*, vol. 5, no. 2, pp. 98–102, Jun. 1995.
[71] M. Esashi, N. Ura, and Y. Matsumoto, "Anodic bonding for integrated capacitive sensors," in *Proc. MEMS*, 1992, pp. 43–48.
[72] H. Henmi, S. Shoji, Y. Yoshimi, and M. Esashi, "Vacuum packaging for microsensors by glass-silicon anodic bonding," *Sens. Actuators A, Phys.*, vol. 43, no. 1–3, pp. 243–248, May 1994.
[73] *Mass Spectral Library*, Nat. Inst. Stand. Technol., Gaithersburg, MD.

**Steven Wright** was born in London, U.K., in 1970. He received the B.Sc. degree in chemistry and the Ph.D. degree in physical chemistry from the University of Southampton, Southampton, U.K., in 1992 and 1996, respectively.

Between 1995 and 2000, he undertook postdoctoral research at the Fritz Haber Institute, Berlin, Germany; Odense University, Odense, Denmark; the University of Duisburg–Essen, Duisburg and Essen, Germany; and the University of Liverpool, Liverpool, U.K. His research interests were in the field of chemical and photochemical reactions on single-crystal surfaces. In 2000, he joined Applied Materials UK Ltd., where he was involved in the development of ion implant systems. He joined Microsaic Systems Ltd., Surrey, U.K., in 2003, where he has been responsible for aspects of mass spectrometer design and development.

**Shane O'Prey** received the B.Sc. degree in pure physics and the Ph.D. degree in physics from Queen's University Belfast, Belfast, U.K., in 1996 and 2002, respectively. The focus of his Ph.D. research was the design and utilization of a system that used surface plasmon resonance effects to investigate the dielectric function of thin-film metals and high-temperature superconducting materials at liquid-nitrogen temperatures.

After several years at Intel Ireland, as a Yield Engineer investigating the root cause of inline defects, he returned to research at Polight Technologies, a Cambridge-based start-up company, developing glass materials for holographic data storage. He joined Microsaic Systems Ltd., Surrey, U.K., in 2005 as a Development Engineer, working extensively on the design and manufacture of MEMS mass spectrometer devices.

**Richard R. A. Syms** (SM'02) received the B.A. degree in engineering science and the D.Phil. degree (on volume holographic optical elements) from Worcester College, Oxford University, Oxford, U.K., in 1979 and 1982, respectively.

He has been the Head of the Optical and Semiconductor Devices Group, Department of Electrical and Electronic Engineering, Imperial College London, London, U.K., since 1992 and Professor of Microsystems Technology since 1996. He has published over 140 journal papers and two books on holography, guided-wave optics, and microengineering. Most recently, he has been developing electrical MEMS such as microconnectors, RF probes for magnetic resonance imaging, and miniature quadrupole mass spectrometers; optical MEMS devices such as alignment devices, variable optical attenuators, and tunable lasers; and three-dimensional self-assembling microstructures. He cofounded the MEMS spin-out company Microsaic Systems Ltd., Surrey, U.K., in 2001.

Dr. Syms is currently an Associate Editor for the JOURNAL OF MICROELECTROMECHANICAL SYSTEMS.

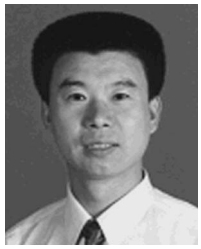

**Guodong Hong** was born in Shandong, China, in 1964. He received the B.Eng. and M.Eng. degrees in material engineering from Shandong University, Jinan, China, in 1984 and 1989, respectively, and the Ph.D. degree in mechanical engineering from Tsinghua University, China, in 1998.

He was a Research Fellow with Nanyang Technological University, Singapore, between 1998 and 2000. Then, he was a Research Associate with Imperial College London, London, U.K., between 2000 and 2004. He joined Microsaic Systems Ltd., Surrey, U.K., in 2005, where he is currently a Product Development Engineer for miniature mass spectrometer design and development.

**Andrew S. Holmes** (M'02) received the B.A. degree in natural sciences from Cambridge University, Cambridge, U.K., in 1987, and the Ph.D. degree in electrical engineering from Imperial College London, London, U.K., in 1992.

He is currently Professor of Microelectromechanical Systems with the Optical and Semiconductor Devices Group, Department of Electrical and Electronic Engineering, Imperial College London. His research interests are mainly in the areas of micropower generation and conversion, MEMS devices for microwave applications, and laser processing for MEMS manufacture. He has been cofounder and Director of Engineering of the MEMS spin-out company Microsaic Systems Ltd., Surrey, U.K., since 2001.